Deconvolution of surface and direct metastable-state blackbody emission in Ti:sapphire laser materials using boxcar time-domain photothermal radiometry

J. Vanniasinkam, A. Mandelis, M. Munidasa, and M. Kokta*

Photothermal and Optoelectronic Diagnostics Laboratories, Department of Mechanical and Industrial Engineering, University of Toronto, Toronto M5S 3G8, Canada

Received May 1, 1997; revised manuscript received August 29, 1997

Single-gate boxcar-integrator time-domain photothermal radiometry (PTR) is proposed as a noncontact remote technique with a high signal-to-noise ratio that can evaluate the optical quality of the surface in a solid-state laser-gain medium such as Ti:sapphire. It was found that immediately after the boxcar-averaged laser-pulse cutoff, the PTR signal is dominated by the laser metastable-level transition lifetime. A PTR theoretical model was formulated to account for this effect and to deconvolute its contribution to the signal from surface absorption of the laser radiation. With the theoretical model, the surface contribution to experimental boxcar PTR signals was deconvoluted and the surface quality was quantified in terms of the surface nonradiative energy generation rate, as the percentage of the input optical power that is converted to heat. © 1998 Optical Society of America [S0740-3224(98)04602-5]

OCIS codes: 120.5630, 350.5340, 140.3380.

1. INTRODUCTION

The primary loss mechanisms in a solid-state laser-gain medium are due to nonradiative energy conversion and spontaneous emission. The production of nonradiative energy in a laser-gain medium is detrimental to the operation of a laser in two ways. First, the more nonradiative energy that is generated, the less energy is available for useful laser output. In addition, this heat dissipation can cause other unwanted effects such as instabilities that are due to thermal birefrengence.[1] The extent to which nonradiative energy is generated in laser materials is highly dependent on the manner in which the laser crystal is grown and on the defects that are present in the crystal.[2] Because the laser material growth process is so essential to the overall efficiency of a solid-state laser, there is a need to develop methods of controlling and evaluating the quality of grown laser crystals.

The nature of the entire crystal growth process (growth, postgrowth annealing, cutting, and polishing) will determine the concentration of defects in the laser crystal and thereby determine its overall laser-output quality. The main purpose of polishing an optical surface is to reduce optical reflection and scattering losses by attempting to remove the small pores, crevasses, grooves, scratches, and cracks present at the unpolished surface.[3] By polishing this surface, it is possible to reduce the characteristic length of such imperfections by an appropriate amount. However, polishing a surface also involves the deposition of impurity inclusions from the polish material to the optical surface. The surface imperfections and impurity inclusions are sites at which optical absorption and nonradiative energy conversion take place. As a result, surfaces with a high density of absorbing sites will exhibit a higher amount of heating.[4]

The method of photothermal radiometry (PTR) involves the detection of infrared emission from a sample that is irradiated by an optical source.[5] The IR emission is related to the sample temperature by the blackbody radiation law. This technique has been recognized as an important tool for the evaluation of bulk thermophysical properties (such as thermal diffusivity and thermal conductivity) of solid samples.[5–7] Several authors[8,9] have presented theoretical treatments of this technique, relating the measured signal to some material parameter. A key requirement of a laser-material evaluation technique is the ability to quantify the extent to which the polished surface acts as a nonradiative energy-conversion site. Improvements in surface preparation technology may produce solid-state laser crystals that outperform the conventional improvements of bulk crystal-growing techniques. In this work, we show that boxcar-integrator-gated time-domain PTR can be used to meet this requirement, subject to the deconvolution of the PTR surface-generated signal from direct spontaneous transitions from the laser metastable level.

2. EXPERIMENT AND RESULTS

A. Experimental Setup

A recent work[10] that presented a theoretical treatment of the temperature response of a solid-state laser material under transient optical excitation predicted that nonradiative processes occurring at the surface and the bulk can be probed and characterized by monitoring the modulated

surface temperature (or alternatively, the modulated IR emission) at early and late times, respectively, after pulse cutoff. Early and late times are labels used in this paper to refer to time ranges that correspond to surface- and bulk-dominated IR emission, respectively. The arrangement of our photothermal radiometric apparatus is shown in Fig. 1. The acousto-optically modulated cw output from an argon-ion laser at the required square-pulse repetition rate and duty cycle impinged on the sample laser-crystal material. Absorption of the incident light and subsequent nonradiative relaxation in the sample resulted in the sample's emitting thermal IR radiation, which was collected and collimated by two off-axis paraboloidal mirrors, which then focused the radiation to an IR detector. The sample response to a square time-gated and boxcar-averaged pulse (incident power, 5 W; spot-size, 100 μm) was used, rather than that to an actual pulsed laser, since the former is mathematically simple for analysis, has a temporal shape that can be precisely controlled, and is of maximum signal-to-noise ratio among time-domain techniques.[11] Pulsed-laser signal averaging may exhibit shot-to-shot variation and jitter and may be the result of irregular pulse time dependencies, thus making mathematical quantitative analysis exceedingly difficult. The PTR signal response increased linearly with the laser irradiance, thus assuring the absence of nonlinear radiometric effects. The detector was a liquid-nitrogen-cooled photoconductive mercury-cadmium-telluride (MCT) detector, with a spectral bandwidth of 2–14 μm. The detector signal was then passed through a preamplifier with a 1-Hz low-frequency cutoff that rejected any dc drift of the MCT detector signal and sent the modulated ac signal to the boxcar integrator, which reconstructs the transient signal by means of a delay sweep of a single time-gate of 100 ns duration. In the experimental configuration of Fig. 1, each data point on a given transient IR-emission profile was obtained as follows. At a given time after the acousto-optically time-gated square-pulse cutoff, each point on the graph represented the average value of the signal measured by the open boxcar gate over 10 000 cycles. The data-acquisition program was written in such a manner that, after 10 000 samples were obtained at one particular location in time, the averaging process over 10 000 cycles would be repeated if the signal-to-noise ratio did not exceed a specified amount. In this case, the preset signal-to-noise ratio was 100 for the early-time measurements. Therefore each point on the transient profile was obtained with a signal-to-noise ratio of at least 100. The result was the reconstruction of the entire PTR signal-decay transient following the square-pulse cutoff, with each point averaged over a span of 10 000 cycles that yielded a signal-to-noise ratio greater than 100.

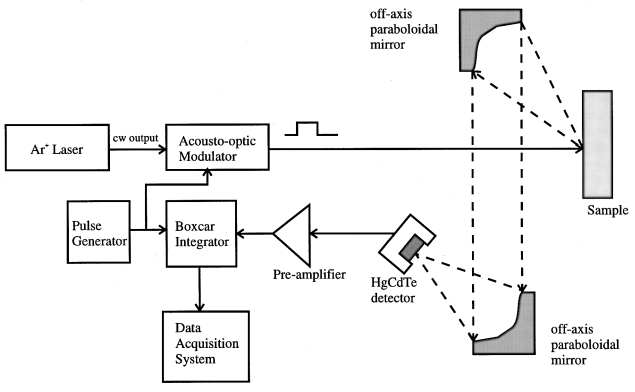

Fig. 1. Experimental layout of a photothermal radiometric-detection system.

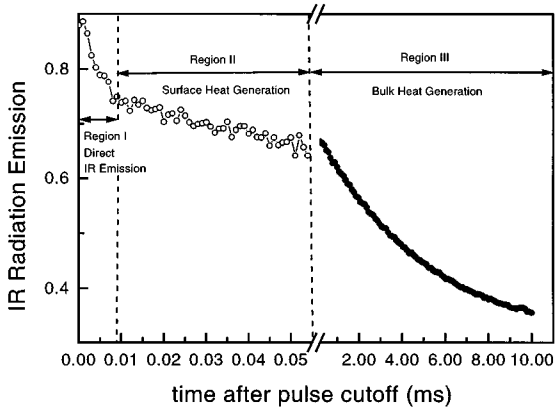

Fig. 2. Three regions of thermal emission: The transient IR-radiation emission signal (normalized to its value at pulse cutoff) is shown in three distinct regions whose profiles are governed by direct IR emission (region I), surface-heat generation (region II), and bulk-heat generation (region III).

B. Identification of Three Regimes of Thermal Emission

Preliminary PTR experiments were conducted to determine and identify the basic features of the transient time-gated IR-emission profiles. The transient IR-emission profile from the time of pulse cutoff to 10 ms later is shown in Fig. 2. From this figure, it was determined that there are three distinct regions of transient decay. Region I is a very steep decay in the 0–10 μs time range. Region II is a much slower decay in the 10–100 μs time range. Region III is a decay in the millisecond range. This bulk-absorption-related region has been studied elsewhere[12] and thus is outside the scope of the present work. The possibility of the decay profile of regions I and II being governed by a single exponential decay was explored. It was determined that the fit of the single exponential decay was not comparable to the fit given by a more complicated expression obtained through physical arguments, which will be explained later. Contrary to the experimental data, the purely conductive model described previously[10] predicts that there are only two distinct regions of temperature decay, which is due to nonradiative energy conversion at the surface and bulk. This disparity implies that the model does not account for the very early (i.e., within one metastable-state decay lifetime) IR-radiation-generating processes that occur in the laser material, since the instrumentation effects have already been accounted for in Fig. 2. These instrumentation effects involve the transfer function of the boxcar integrator and are accounted for by short circuiting the inputs to the boxcar integrator and obtaining a transient profile. This profile is then subtracted from the IR-emission signal, thereby accounting for the instrumental

impulse response. The original assumption made in the derivation of the PTR theory in Ref. 10 was that the sample was opaque to its own radiation within the spectral range corresponding to the spectral bandwidth of the IR detector. A Fourier-transform IR-transmittance spectrum of a Ti:sapphire crystal in the 2–25-μm range showed, however, that the sample was not opaque in the $\leqslant$ 6-μm range. It is therefore possible that any IR radiation in the 2–6-μm range generated in the sample might not be reabsorbed by the sample and would therefore be collected by the detector. Comparison of the experimental data and theoretical predictions lead to the conclusion[10,12] that region II is due to surface-heating effects, and region III is due to bulk-heating effects, leaving region I as the region in which the source of the signal was as yet unaccounted for.

C. Origins of Thermal Emission in 0–5-μs Range

To determine the origin of the IR emission shown in region I of Fig. 2, which is not yet accounted for, two experiments were conducted in which decay transients were obtained with widely different pump-photon energies above and below the electronic threshold in Ti:sapphire. In view of the Fourier-transform IR-transmittance spectrum, photons emitted in the $\leqslant$ 6-μm range will be transmitted through and out of the sample and collected by the detector, generating the decay profile shown in region I of Fig. 2. To confirm that excited-state ions are indeed responsible for this direct emission, instead of the argon-ion laser, a Nd:YAG pump laser emitting at the 1.06-μm wavelength was used. At such a wavelength, there is not enough photon energy to excite the crystal dopants to the $2E$ excited state,[13] thereby ensuring that the observed PTR signals would not originate at the Ti^{3+} ion metastable laser level. As a result, no IR photons should be emitted, and the decay characteristic of region I should be absent. Figure 3 shows the PTR signal for the Nd:YAG-pumped Ti:sapphire laser material. The break in the transient profile at about 10 μs after pulse cutoff is not present in this curve, as expected. The above two experiments confirm that the signal in region I is a radiative process from the excited upper laser level.

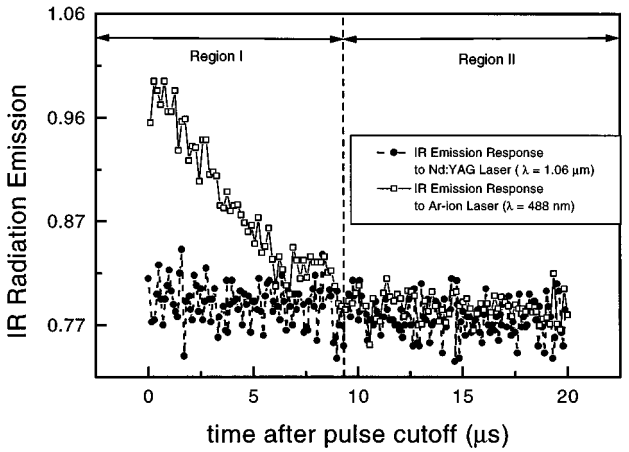

Fig. 3. Comparison of the radiation-emission transient from a laser material in response to argon-ion laser excitation and Nd:YAG laser excitation. The early-time fast decay seen with argon-ion laser excitation in the 0–10-μs range is not present with the Nd:YAG excitation. Detector bandwidth is 2 to 14 μm. The y axis represents the IR emission, normalized to its value at pulse cutoff.

As a result of this additional component to the experimental signal, which was not accounted for in the theoretical model developed earlier,[10] a model generalization is required to quantify the direct IR-emission component of the radiation-emission signal.

3. EARLY-TIME THEORETICAL MODEL

A model of the PTR signal valid for the early times (i.e., commensurate with the metastable-state lifetime) after a square-pulse cutoff is presented here. At such early times (typically 0–100 μs for Ti:sapphire), two contributions to the IR-emission signal are assumed to be present. The first contribution is IR-photon emission by spatially stationary photoexcited Ti^{3+} ions, followed immediately by a contribution that is due to the nonradiative power-conversion processes occurring at the surface of the crystal. Any contributions to the IR-emission signal that are due to nonradiative processes occurring in the bulk of the crystal are ignored to keep the theory relatively simple, since the time ranges of these processes are much longer (of the order of milliseconds).

Consider a laser rod of length L with its front surface labeled by $z = 0$. For repetitive (periodic) optical excitation, the IR-absorption coefficient of a Ti:sapphire laser rod is

$$\beta_{\mathrm{IR}}(z, t; \lambda) = \beta_{\mathrm{IR}}^{(o)}(z; \lambda) + \Delta\beta_{\mathrm{IR}}(z, t; \lambda), \qquad (1)$$

where $\beta_{\mathrm{IR}}^{(o)}(z; \lambda)$ is the background IR-absorption coefficient in the absence of a pump laser beam and $\Delta\beta_{\mathrm{IR}}(z, t; \lambda)$ is the time-dependent IR-absorption coefficient that is due to optical transitions of spatially stationary photoexcited Ti^{3+} ions. In the above equation $(z, t; \lambda)$ are the depth coordinate, time coordinate, and IR wavelength, respectively. Let T_∞ be the ambient temperature and $\theta(z, t)$ be the time-dependent temperature change at the center of the Gaussian laser-beam profile as it propagates through the crystal, which is due to absorption by the sample. Planck's distribution function is given by

$$W_P(\lambda, \theta_T; z) = \frac{2\pi hc^2 A}{\lambda^5\left\{\exp\left[\dfrac{hc}{\lambda k_B \theta_T(z, t)}\right] - 1\right\}}, \qquad (2)$$

where $\theta_T(z, t) = T_\infty + \theta(z, t)$ is the absolute temperature of the sample, A is the emitting surface area, k_B is Boltzmann's constant, h is Planck's constant, and c is the speed of light. The change in Planck's distribution function $W_P(\lambda, \theta_T; z)$ can be found by expanding this function around $\theta_T = T_\infty$ with a Taylor series expansion, keeping the first (linear) term in accordance with the linearity of our experiments, and making the definition

$$\Delta W_P[\lambda, \theta_T = T_\infty + \theta(z, t)] \equiv \left[\left.\frac{\partial W_P}{\partial \theta_T}\right|_{\theta_T = T_\infty}\right]\theta(z, t). \qquad (3)$$

Upon differentiating W_P and setting the product $\theta(\partial W_P/\partial\theta_T)|_{\theta_T=T_\infty}$ equal to a quantity $\Delta W_P(\lambda, T_\infty)$, Eq. (3) becomes

$$\Delta W_P(\lambda, T_\infty; z, t) = \left(\frac{hc}{\lambda k_B T_\infty}\right) W_P(\lambda, T_\infty) \frac{\exp(hc/\lambda k_B T_\infty)}{\exp(hc/\lambda k_B T_\infty) - 1}\left[\frac{\theta(z, t)}{T_\infty}\right]. \quad (4)$$

One can now rewrite Planck's distribution function to first order in the Taylor expansion

$$W_P[\lambda, \theta_T(z, t)] \approx W_P(\lambda, T_\infty) + \Delta W_P(\lambda, T_\infty; z, t). \quad (5)$$

To calculate the IR radiation that is incident on the MCT detector, the first step is to find the total IR-radiation power (power unit wavelength) arriving at the surface of the material from the interior. This quantity, integrated over the spectral bandwidth of the detector and adjusted for reflection losses at the inner-front surface of the crystal, will yield the power incident on the detector. The total IR-radiation power (per unit wavelength) at the surface of the material arriving from the interior of a laser rod of length L is

$$P(\lambda, t) = \int_0^L \beta_{\mathrm{IR}}(z, t; \lambda)\exp\left[-\int_0^z \beta_{\mathrm{IR}}(z', t; \lambda)\mathrm{d}z'\right] \times \Delta W_P[\lambda, \theta_T(z, t)]\mathrm{d}z. \quad (6)$$

Using Eqs. (1), (3), and (5), the above equation can be expanded to

$$P(\lambda, t) = \int_0^L [\beta_{\mathrm{IR}}{}^{(o)}(z; \lambda) + \Delta\beta_{\mathrm{IR}}(z, t; \lambda)][W_P(\lambda, T_\infty) + \Delta W_P(\lambda, T_\infty; z, t)] \times \exp\left\{-\int_0^z [\beta_{\mathrm{IR}}{}^{(o)}(z'; \lambda) + \Delta\beta_{\mathrm{IR}}(z', t; \lambda)]\mathrm{d}z'\right\}\mathrm{d}z. \quad (7)$$

One can also set

$$\int_0^z \beta_{\mathrm{IR}}{}^{(o)}(z'; \lambda)\mathrm{d}z' = \beta_{\mathrm{IR}}{}^{(o)}(\lambda)z, \quad (8)$$

since the background IR-absorption profile across the thickness of the crystal in the absence of optical excitations is expected to be reasonably homogeneous. The rise in the IR-absorption coefficient (which is equal to the IR-emission coefficient by Kirchoff's law of detailed balance) is spatially dependent on and proportional to the density of the photoexcited Ti^{3+} ions. For typical doping concentrations of the host crystal of $\sim 0.1\%$, the density of Ti^{3+} ions is negligible, implying

$$\int_0^L \Delta\beta_{\mathrm{IR}}(z, t; \lambda)\mathrm{d}z' \ll 1. \quad (9)$$

As a result of Eq. (8) and inequality (9),

$$\exp\left\{-\int_0^L [\beta_{\mathrm{IR}}{}^{(o)}(z'; \lambda) + \Delta\beta_{\mathrm{IR}}(z, t; \lambda)]\mathrm{d}z'\right\} \approx \exp[-\beta_{\mathrm{IR}}{}^{(o)}z]. \quad (10)$$

Equation (7) may be written as a summation of four integrals,

$$\begin{aligned} P(\lambda, t) = {} & \int_0^L \beta_{\mathrm{IR}}{}^{(o)}(z; \lambda)W_P(\lambda, T_\infty) \times \exp[-\beta_{\mathrm{IR}}{}^{(o)}z]\mathrm{d}z \\ & + \int_0^L \beta_{\mathrm{IR}}{}^{(o)}(z; \lambda)\Delta W_P(\lambda, T_\infty; z, t) \times \exp[-\beta_{\mathrm{IR}}{}^{(o)}z]\mathrm{d}z \\ & + \int_0^L \Delta\beta_{\mathrm{IR}}(z, t; \lambda)W_P(\lambda, T_\infty) \times \exp[-\beta_{\mathrm{IR}}{}^{(o)}z]\mathrm{d}z \\ & + \int_0^L \Delta\beta_{\mathrm{IR}}(z, t; \lambda)\Delta W_P(\lambda, T_\infty; z, t) \times \exp[-\beta_{\mathrm{IR}}{}^{(o)}z]\mathrm{d}z, \end{aligned} \quad (11)$$

where the first term is independent of time and represents the background radiation level on which the pump-laser-induced radiometric transient is superposed. The last term includes the product of two small quantities, ΔW_P and $\Delta\beta_{\mathrm{IR}}$, and is therefore negligible compared with the second and third terms in the above equation. Because the boxcar integrator filters out any dc components of the measured signal, neglecting the first (constant) term as well as the last (second-order) term and rewriting the above equation gives for the transient part of Eq. (11)

$$\begin{aligned} P(\lambda, t) \approx {} & \int_0^L \beta_{\mathrm{IR}}{}^{(o)}(z; \lambda)\Delta W_P(\lambda, T_\infty; z, t) \times \exp[-\beta_{\mathrm{IR}}{}^{(o)}z]\mathrm{d}z \\ & + \int_0^L \Delta\beta_{\mathrm{IR}}(z, t; \lambda)W_P(\lambda, T_\infty) \times \exp[-\beta_{\mathrm{IR}}{}^{(o)}z]\mathrm{d}z. \end{aligned} \quad (12)$$

Under Kirchhoff's law of detailed balance, this equation gives a clear indication that the measured experimental signal will be due to a change in the thermal emission ΔW_p and a change in the direct excited-state emission $\Delta\beta_{\mathrm{IR}}$. In the above equation, $\Delta\beta_{\mathrm{IR}}$ is proportional to the distribution of stationary IR-photon-absorbing Ti^{3+} ions and is given by

$$\Delta\beta_{\mathrm{IR}}(z, t; \lambda) = (1 - \Gamma_s)\sigma_{\mathrm{IR}}N_2(t)\exp(-\beta_{\mathrm{vis}}z), \quad (13)$$

where $N_2(t)$ is the time-dependent population of the metastable state in Ti:sapphire. σ_{IR} is the absorption cross section, β_{vis} is the absorption coefficient of the pump wavelength, and Γ_s is the surface absorptance. Recalling that $\beta_{\mathrm{IR}}{}^{(o)}$ is independent of the depth coordinate and substituting Eqs. (4) and (13) into Eq. (12), one obtains

$$P(\lambda, t) = W_P(\lambda, T_\infty) \times \left\{ \frac{hc\beta_{\mathrm{IR}}^{(o)}\exp(hc/\lambda k_B T_\infty)}{\lambda k T_\infty^2\left[\exp\left(\frac{hc}{\lambda k_B T_\infty}\right) - 1\right]} \times \int_0^L \theta(z, t)\exp[-\beta_{\mathrm{IR}}^{(o)} z]\mathrm{d}z + \sigma_{\mathrm{IR}}\int_0^L N_2(t)\exp(-\beta_T z)\mathrm{d}z \right\}, \quad (14)$$

where $\beta_T = \beta_{\mathrm{vis}} + \beta_{\mathrm{IR}}^{(o)}$. For long crystal rods, one assumes $L \to \infty$, and Eq. (14) becomes

$$P(\lambda, t) = W_P(\lambda, T_\infty)\left\{ a(\lambda)\int_0^\infty \theta(z, t)\exp[-\beta_{\mathrm{IR}}^{(o)} z]\mathrm{d}z + b(\lambda)N_2(t)\right\}, \quad (15)$$

where

$$a(\lambda) \equiv \frac{hc\beta_{\mathrm{IR}}^{(o)}\exp(hc/\lambda k_B T_\infty)}{\lambda k_B T_\infty\left[\exp\left(\frac{hc}{\lambda k_B T_\infty}\right) - 1\right]},$$

$$b(\lambda) \equiv \frac{\sigma_{\mathrm{IR}}}{\beta_T(\lambda_{\mathrm{vis}})}.$$

This expression for $P(\lambda, t)$ is the total transient IR-radiation power (per unit wavelength) at the surface of the material. Using $P(\lambda, t)$, the IR emission collected by the MCT detector, accounting for reflection losses, and integrating over the bandwidth $\lambda_1 - \lambda_2$ of the detector, we obtain

$$S(t; \lambda_{\mathrm{vis}}) = [1 - R(\lambda_{\mathrm{vis}})]\int_{\lambda_1}^{\lambda_2}[1 - R(\lambda)]P(\lambda, t)\mathrm{d}\lambda. \quad (16)$$

Incorporating Eq. (15) into the above equation and rearranging yields

$$S(t; \lambda_{\mathrm{vis}}) = A(\lambda_{\mathrm{vis}})\int_0^\infty \theta(z, t) \times \exp[-\beta_{\mathrm{IR}}^{(o)} z]\mathrm{d}z + B(\lambda_{\mathrm{vis}})(1 - \Gamma_S)N_2(t), \quad (17)$$

where $A(\lambda_{\mathrm{vis}}) \equiv [1 - R(\lambda_{\mathrm{vis}})]\int_{\lambda_1}^{\lambda_2}[1 - R(\lambda)]W_P(\lambda, T_\infty) \times a(\lambda)d\lambda$ and $B(\lambda_{\mathrm{vis}}) \equiv [1 - R(\lambda_{\mathrm{vis}})]\int_{\lambda_1}^{\lambda_2}[1 - R(\lambda)] \times W_P(\lambda, T_\infty)b(\lambda)d\lambda$. The second term in Eq. (17) is responsible for direct emission from the metastable upper laser level and represents the modification of the earlier model[10] to include this effect. The first term in Eq. (17) represents an additional extension to Ref. 10 in taking into account the nonopacity of the laser material to the emitted IR radiation. $\theta(z, t)$ is as derived earlier.[10] Under experimental conditions, the terms $A(\lambda_{\mathrm{vis}})$ and $B(\lambda_{\mathrm{vis}})$ can be considered as multiplicative constants in Eq. (17). Next, one must evaluate the integral $\int_0^\infty \theta(z, t)\exp[-\beta_{\mathrm{IR}}^{(o)} z]dz$. $\theta(z, t)$ can be obtained from expressions evaluated at very early times,[10] when heat conduction to the crystal surface from volume sources (bulk) can be neglected. In addition, the characteristic thermal transfer time τ_h from the surface to the surroundings by means of radiation or convection heat transfer is assumed to be much longer than the observation time interval, and radial heat flow is also considered to be negligible in that observation time interval. The integral $\int_0^\infty \theta(z, t)\exp[-\beta_{\mathrm{IR}}^{(o)} z]dz$ can then be written explicitly as[10]

$$I(t) = \frac{2I_0\Gamma_S\alpha}{\pi k} \times \begin{cases} \left\{ 2\sqrt{\frac{\tau_{\mathrm{IR}}}{\pi}}\,t - \tau_{\mathrm{IR}}\left[1 - Y\left(\sqrt{\frac{\tau}{\tau_{\mathrm{IR}}}}\right)\right]\right\} & \text{if } t < \tau_p \\ \int_0^{\tau_p} Y[\beta_{\mathrm{IR}}^{(o)}\sqrt{\alpha(t - t_0)}]\mathrm{d}t_0 & \text{if } t > \tau_p \end{cases}, \quad (18)$$

where $\tau_{\mathrm{IR}} \equiv 1/\{[\beta_{\mathrm{IR}}^{(o)}]^2\alpha\}$, $Y(x) \equiv \exp(x^2)\mathrm{erfc}(x)$, α is the thermal diffusivity, and k is the thermal conductivity. τ_{IR} is the characteristic photothermal time for heat conduction to the surface from a depth equal to the IR optical-absorption length. It is based on the IR-absorption coefficient and the thermal diffusivity of the sample. Finally, Eq. (18) is substituted into Eq. (17), yielding the desired expression for the IR emission collected by the detector immediately after pulse cutoff and for times short compared with the bulk thermal transport time (of the order of milliseconds) from a depth equal to the optical absorption length, $\beta_{\mathrm{vis}}^{-1}$, at the pump laser wavelength:

$$S(t > \tau_p; \lambda_{\mathrm{vis}}) = (1 - \Gamma_s)B(T_\infty, \lambda_{\mathrm{vis}})W_{po}N_T\tau \times [\exp(\tau_p/\tau_{21}) - \exp(-W_{po}\tau_p)] \times \exp(-t/\tau_{21}) + \frac{2A(T_\infty, \lambda_{\mathrm{vis}})I_0\Gamma_S\alpha\tau_{\mathrm{IR}}}{\pi k} \times \left[Y\left(\sqrt{\frac{t}{\tau_{IR}}}\right) - Y\left(\sqrt{\frac{t - \tau_p}{\tau_{\mathrm{IR}}}}\right) + \frac{2}{\sqrt{\pi\tau_{\mathrm{IR}}}}(\sqrt{t} - \sqrt{t - \tau_p})\right], \quad (19)$$

where τ is defined as

$$\frac{1}{\tau} \equiv \frac{1}{\tau_{21}} + W_{po}, \quad (20)$$

and W_{po} is the pump-laser-beam-induced optical excitation rate. Since only the decay of the transient acousto-optically time-gated profile is being monitored, only the $t > \tau_p$ regime is of interest here. The first term of the above equation represents the direct IR emission by stationary excited Ti^{3+} ions along the axis $r = 0$ of the depth coordinate z in the crystal. This term is responsible for the early fast decay of the signal shown in region I of Fig. 2 and has been shown to have a similar functional form as the luminescence transient measured by a photodiode.

Table 1. Explanation of Variables Used in the Early-Time Eq. (19)

Parameter	Method of Determination	Value
Surface absorptance, Γ_s	From curve fitting	To be obtained
Spectrally integrated constants A, B	A, B same for all samples	Not required
Characteristic time, τ_{IR}	FTIR absorption spectra	12 s
Thermal conductivity, k	Literature[16]	33 W/(mK)
W_{po}, N_T, τ, τ_{21}	From luminescence curve fits	Sample dependent
Thermal diffusivity α	Literature[16]	0.106 cm^2/s

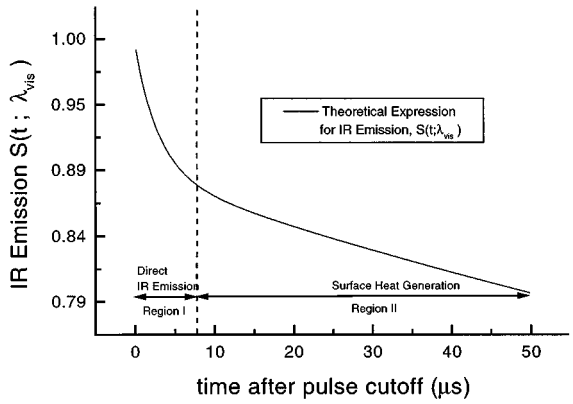

Fig. 4. A plot of the predicted transient IR emission in the early-time range. Parameters used can be found in Table 1. The y axis represents the IR emission, normalized to its value at pulse cutoff.

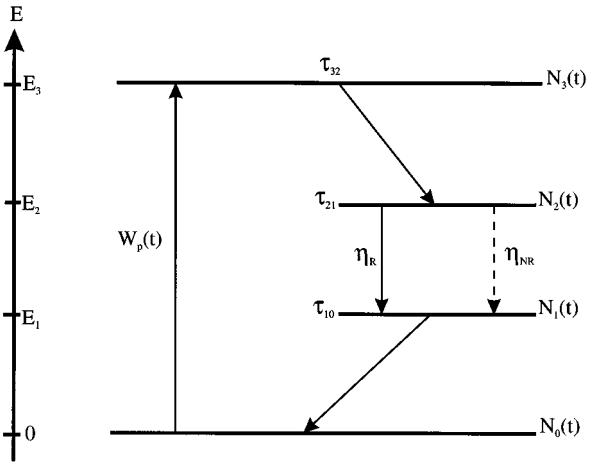

Fig. 5. Energy level diagram of a four-level laser system. $N_j(t)$, population of level $|j\rangle$; τ_{jk}, total lifetime of level $|j\rangle$ undergoing transition to level $|k\rangle$; η_R (η_{NR}), radiative (nonradiative) quantum yield of metastable level $|2\rangle$; $W_p(t)$, ground-state pumping rate.

The second term represents the IR-radiation emission that is due to nonradiative processes occurring at the surface, represented by region II of Fig. 2. In the above equation, A and B are independent of time but depend on temperature and on the spectral range of the detector. Γ_S, the important surface absorptance parameter, is found by fitting Eq. (19) to the experimental data. The parameters involved in Eq. (19) are shown in Table 1. A plot of the theoretical (predicted) transient IR emission collected by the detector, given by Eq. (19) in the early-time range, is shown in Fig. 4, where the two distinct regions of emission can be seen.

4. DATA ANALYSIS AND DISCUSSION

The surface quality of several Ti:sapphire laser materials was characterized by boxcar time-domain PTR in the following manner. For a given sample, the transient luminescence signal was measured, from which the upper-laser-level lifetime τ_{21} was obtained, shown simplified in Fig. 5. The PTR signal-decay early-time region yields information about direct excited-state emission and surface nonradiative energy conversion as a result of fitting the early-time PTR experimental data to Eq. (19). From the curve fit, one obtains fitting parameters that represent the nonradiative surface power generation and the efficiency of direct emission.

If we rewrite Eq. (19) compactly in the form

$$S(t;\lambda_{\mathrm{vis}}) = \phi_1\tau[\exp(\tau_p/\tau_{21}) - e(-W_{po}\tau_p)]\exp(-t/\tau_{21}) + \phi_2\left[Y\left(\sqrt{\frac{t}{\tau_{\mathrm{IR}}}}\right) - Y\left(\sqrt{\frac{t-\tau_p}{\tau_{\mathrm{IR}}}}\right) + \frac{2}{\sqrt{\pi\tau_{\mathrm{IR}}}}(\sqrt{t} - \sqrt{t-\tau_p})\right], \quad (21)$$

where the two fitting parameters are

$$\phi_1 = (1-\Gamma_s)B(T_\infty, \lambda_{\mathrm{vis}})W_{po}N_T, \quad (22)$$

$$\phi_2 = \frac{2A(T_\infty, \lambda_{\mathrm{vis}})I_o\Gamma_S\alpha\tau_{\mathrm{IR}}}{\pi k}, \quad (23)$$

the curve-fitting process for the early-time data results in the determination of the two fitting parameters, ϕ_1 and ϕ_2, for a given crystal. In the expressions for ϕ_1 and ϕ_2, the only quantity that varies from crystal to crystal is the surface absorptance, Γ_s. The other quantities such as k (thermal conductivity), α (thermal diffusivity), W_{po} (pumping rate), N_T (total population) and I_o (optical intensity) can be assumed constant from sample to sample, given identical input pumping conditions. The surface reflectivity of polished Ti:sapphire crystals has been measured[14] and found to be $<8\%$ and spectrally flat in the 400–1000-nm range. Therefore it was neglected in expressions (22) and (23). Also, A and B are constant from sample to sample, since these two parameters are multiplicative constants that depend only on ambient temperature and the spectral range of the detector.

For a given crystal sample i, the curve-fitting routine returns values of ϕ_1 and ϕ_2. Then Eq. (22) and (23) are rewritten as $\phi_1^{(i)} = K_1(1-\Gamma_s^i)$ and $\phi_2^{(i)} = K_2\Gamma_s^i$, where

K_1 and K_2 are the same for all crystal samples. Finally, the surface nonradiative energy generation rate, Q_s is defined as

$$Q_s = I_o \Gamma_s (\mathrm{W/m^2}), \tag{24}$$

where I_o is the incident laser irradiance and Γ_s is the surface absorptance. In the evaluation of the experimental results, the surfaces of different crystals are characterized by the Q_s parameter, which is obtained using Γ_s from the results of the curve fitting to experimental data.

A. Analysis of Ti:Sapphire Samples

1. Ti:Sapphire Sample with an Unpolished Surface

This sample was a Czochralski-grown crystal that had not been subjected to any surface polishing. This crystal was used as a coarse reference to give some indication of the very small differences in surface quality of other, laser-quality crystals.

2. Samples of Different Bulk Quality but Identical Surface Quality

This set of samples consisted of a low-bulk-quality figure of merit (FOM = 40) and a high-bulk-quality figure of merit (FOM = 800), whose differences in bulk optical quality were due to differences in growth processes. The two crystals were grown in an identical manner using the Czochralski technique, following which the FOM = 800 sample was subjected to further annealing, thereby removing bulk defects present in the crystal.[15] The FOM parameter represents the ratio of the absorption coefficient at the absorption peak to the absorption coefficient at the emission peak of Ti:sapphire, $\beta_{488\,\mathrm{nm}}/\beta_{800\,\mathrm{nm}}$. A high FOM implies a high-quality bulk, since the residual absorptions at the emission wavelength $\beta_{800\,\mathrm{nm}}$ will be much lower for an annealed crystal. The two samples were then subjected to the same surface-treatment procedure. The surface processing consisted of mechanical polishing using a diamond paste containing 5-μm particulates.

3. Samples of Identical Bulk Quality but Different Surface Quality

Two samples were used, both of high-bulk-quality FOM, implying that they have both been subjected to the same growth procedure and also to postgrowth annealing, whose surfaces had been treated with two different polishes. One crystal was polished with the best available surface polish, consisting of mechanical polishing using a diamond paste containing 1-μm particulates followed by mechanical polishing using 0.25-μm diamond particulates. The other crystal was polished with a diamond paste containing 5-μm particulates.

B. Surface Characterization Using Photothermal Radiometric Signal Deconvolution

With the curve-fitting routine mentioned earlier, the experimental data were fitted to the theoretical expression for the IR-radiation emission given by Eq. (21).

The low (FOM = 40) and high (FOM = 800) bulk-quality figure-of-merit crystals had surfaces polished in exactly the same manner. The radiometric emission transient profiles of these two samples are shown in Fig. 6. As seen here, the transient signal evolution of the two crystals shows almost overlapping behavior. Following pulse cutoff, region I shows a steep decay that is due to direct IR emission by Ti^{3+} ions in the excited state. This decay is governed by the radiative lifetime of the crystal. The two curves overlap at early times <10 μs because their radiative lifetimes are very similar, as verified by luminescence lifetime measurements. Region II shows two curves with a much slower decay rate governed by the IR-photon emission by the sample due to nonradiative processes occurring at the crystal surface. One expects the nonradiative processes occurring at the crystal surface to be very similar for both samples, since both samples have been subjected to the same surface treatment. As a result, the transient profiles in region II are very similar for both samples, as shown in Fig. 6.

To quantify the effects of the nonradiative processes occurring at the surfaces of the two materials, the experimental transient profiles are fitted to Eq. (21), yielding the fitting parameters ϕ_1 and ϕ_2 [Eqs. (22) and (23)] and subsequently Q_s. For these two samples $Q_s = 0.234 I_o(\mathrm{W/cm^2})$ for the low FOM = 40 crystal and $Q_s = 0.229 I_o(\mathrm{W/cm^2})$ for the high FOM = 800 crystal. A more physically meaningful way of expressing these results is to state that the FOM = 40 crystal has a surface that converts 23.4% of the input optical irradiance to heat and the FOM = 800 crystal has a surface that converts 22.9% of the input optical irradiance to heat.

Next, the two crystals with similar bulk properties whose surfaces had been treated differently were studied to test the applicability of the signal deconvolution operation, with the aim of determining whether the boxcar-averaged time-domain PTR detection in the early-time (microsecond) range is sensitive enough to detect the differences in the nonradiative energy generation at these two crystal surfaces as a result of the differences in surface polishing. Figure 7 shows the transient IR-emission profile for the two crystals. In region I, the two curves overlap since the two crystals have similar radiative lifetimes as verified by luminescence experiments. In region

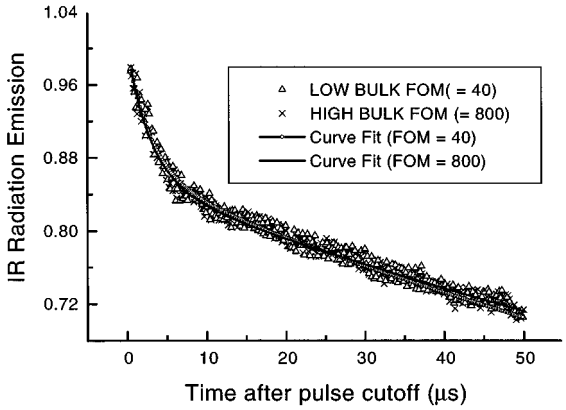

Fig. 6. IR-radiation-emission boxcar transient (normalized to its value at pulse cutoff) from a high-FOM and a low-FOM crystal with the same surface polish, measured in the early-time microsecond range where bulk effects are not important. Detector bandwidth is 2 to 14 μm. $\tau_{21} = 3.01$ μs for the FOM = 40 crystal and 2.99 μs for the FOM = 800 crystal, measured independently through luminescence experiments.

II, the crystal with the 5-μm polished surface decays faster than the crystal with the 0.25-μm polished surface. To put the sensitivity of this technique in perspective regarding its ability to detect minute differences in surface quality, the differences in the radiation-emission signal of the 0.25-μm polished crystal and the 5-μm polished crystal shown in Fig. 7 were compared with the emission signal obtained from the unpolished crystal. This comparison is shown in Fig. 8, where it is noted that the differences in the 0.25-μm polished crystal and the 5-μm polished crystal are indeed very small when compared with the unpolished crystal. This figure indicates the dynamic range and sensitivity the detection technique should possess to detect changes in different grades of industrial-quality polish processing techniques.

To quantify the differences in surface polish quality of these two crystals, the deconvolution Eq. (21) was used to obtain the fitting parameters, which ultimately yield the values of Q_s. The value of the excited-state lifetime was obtained from the slope of the early (steep) decay profile

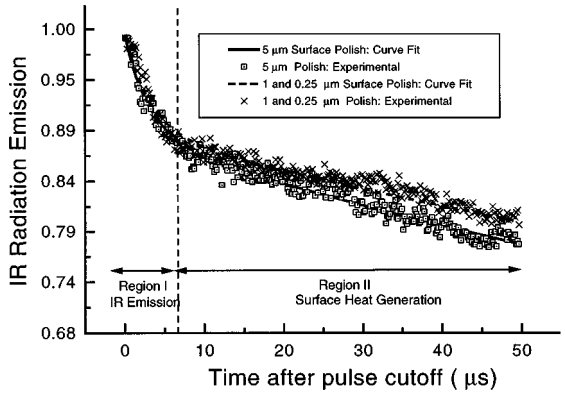

Fig. 7. IR-radiation-emission boxcar transient (normalized to its value at pulse cutoff) from a 5-μm polished surface and a 0.25-μm polished surface of two Ti:sapphire crystals of the same bulk FOM, measured in the early-time microsecond range where bulk effects are absent and surface effects dominate. Detector bandwidth is 2 to 14 μm. $\tau_{21} = 2.61$ μs for the crystal with the 0.25-μm polished surface and 2.56 μs for the crystal with the 5-μm polished surface, measured independently through luminescence experiments.

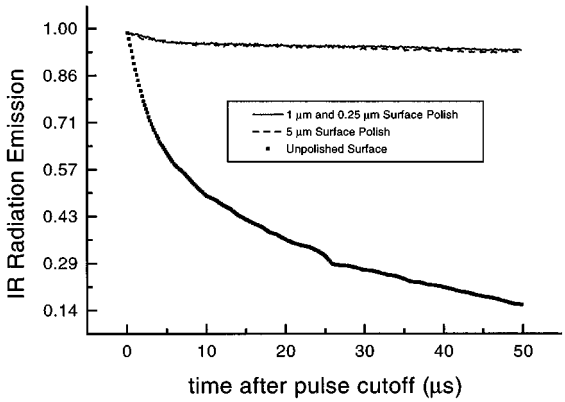

Fig. 8. Comparison of IR-radiation-emission profiles (normalized to their values at pulse cutoff) of the two laser-quality polished samples of Fig. 7 with an unpolished crystal. Detector bandwidth is 2 to 14 μm.

and was found to be consistent with independent luminescence measurement. Furthermore, the fits yield $Q_s = 0.238 I_o(\mathrm{W/cm^2})$ for the 5-μm polished surface and $Q_s = 0.180 I_o[\mathrm{W/cm^2}]$ for the 0.25-μm polished surface. The unpolished sample decay curve could not be treated by the signal deconvolution formalism presented in this paper. Nevertheless, it could be fitted to a purely surface-generated semi-infinite thermal conduction transient,[10] reflecting the substantial thickness of the surface damage layer acting as a 100% optical-to-thermal energy-conversion site.

In evaluating the surface quality of the 0.25-μm polished surface and the 5-μm polished surface, it was found that the surface nonradiative energy-generation rate Q_s is 32% higher for the 5-μm polished surface. This trend is to be expected because the finer the grit size of the polishing material, the lower the minimum size of the imperfections or defects that can be removed, which are optically absorbing sites at the surface of the material. Therefore the number of absorbing (and heat-producing) sites is greater on the 5-μm polished surface than on the 0.25-μm polished surface, resulting in a greater value of Q_s for the 5-μm polished surface. In evaluating the surface properties of the FOM = 40 and FOM = 800 crystals (both having 5-μm polished surface), Q_s values were found to be within 2% of each other. This difference of 2% between the two identically processed surfaces is not significant because the difference falls within the value of the 5% error tolerated by the curve-fitting routine.

The current methods of laser-crystal surface-quality inspection in manufacturing environments rely heavily on visual inspection along with scratch-and-dig specifications, knowledge of polishing process (since the depth of subsurface damage is directly dependent on particle sizes of an abrasive), and optical illumination and magnification instruments. Although techniques such as atomic-force microscopy can provide surface-roughness measurements at the angstrom level, such techniques are not practical in a production environment. In view of these facts, photothermal radiometry is a laser-crystal surface-characterization technique that advances the state of the art in that it can both distinguish between two almost identical laser-crystal surfaces and be easily integrated into the laser-crystal production process owing to its noncontact, remote nature.

5. CONCLUSIONS

The PTR time-domain boxcar detection technique can monitor nonradiative processes at laser-material surfaces by detecting the IR emission from the material several microseconds after pulse cutoff. The early-time PTR technique can successfully deconvolute the direct excited metastable-state emission contribution to the PTR signal from that due to minute surface absorptions. Furthermore, the almost identical values of Q_s for the two crystals of different bulk quality confirm that early-time PTR detection is entirely insensitive to any bulk differences and can be used to monitor the optical quality of Ti:sapphire crystal surfaces through their efficiency as nonradiative power-conversion sites. These conclusions complement earlier results,[12] which showed that PTR can also

monitor nonradiative processes within the laser-crystal bulk by detecting the IR emission from the crystal several milliseconds after pulse cutoff. At these late times, the heat generated in the bulk will dominate the total IR-emission signal, and PTR was found to be insensitive to any changes in nonradiative surface processes that might be occurring.

ACKNOWLEDGMENTS

The authors acknowledge the support of the Natural Sciences and Engineering Research Council of Canada and the Materials and Manufacturing Ontario throughout the duration of this project.

M. Kokta is also with Union Carbide, Inc., Washougal, Washington.

REFERENCES

1. W. Koechner, *Solid State Laser Engineering*, 3rd ed. (Springer-Verlag, New York, 1992).
2. J. F. Pinto, L. Esterowitz, G. H. Rosenblatt, M. Kokta, and D. Peressini, "Improved Ti:sapphire laser performance with new high figure of merit crystals," IEEE J. Quantum Electron. **30**, 2612–2616 (1994).
3. N. Bloembergen, "Role of cracks, pores, and absorbing inclusions on laser induced damage threshold at surfaces of transparent dielectrics," Appl. Opt. **12**, 661–664 (1973).
4. W. Lowdermilk and D. Milam, "Laser-induced surface and coating damage," IEEE J. Quantum Electron. **17**, 1888–1903 (1981).
5. P. E. Nordal and S. O. Kanstad, "New developments in photothermal radiometry," Infrared Phys. **25**, 295–304 (1985).
6. A. C. Tam, "Pulsed photothermal radiometry for noncontact spectroscopy, material testing and inspection measurements," Infrared Phys. **25**, 305–313 (1985).
7. W. P. Leung and A. C. Tam, "Techniques of flash radiometry," J. Appl. Phys. **56**, 153–161 (1984).
8. R. D. Tom, E. P. O'Hara, and D. Benin, "A generalized model of photothermal radiometry," J. Appl. Phys. **53**, 5392–5400 (1982).
9. R. Santos and L. C. M. Miranda, "Theory of the photothermal radiometry with solids," J. Appl. Phys. **52**, 4194–4198 (1981).
10. A. Mandelis and J. Vanniasinkam, "Theory of nonradiative decay dynamics in solid-state laser media via laser photothermal diagnostics," J. Appl. Phys. **80**, 6107–6119 (1996).
11. A. Mandelis, "Signal-to-noise ratio in lock-in amplifier synchronous detection: a generalized communications systems approach with applications to frequency, time, and hybrid (rate window) photothermal measurements," Rev. Sci. Instrum. **65**, 3309–3323 (1994).
12. J. Vanniasinkam, M. Munidasa, A. Othonos, M. Kokta, and A. Mandelis, "Diagnostics of nonradiative defects in the bulk and surface of brewster-cut Ti:sapphire laser materials using photothermal radiometry," IEEE J. Quantum Electron. **33**, 2301–2310 (1997).
13. B. F. Gachter and J. A. Koningstein, "Zero phonon transitions and interacting Jahn-Teller phonon energies from the fluorescence spectrum of Ti:sapphire," J. Chem. Phys. **60**, 2003–2006 (1974).
14. J. Vanniasinkam, A. Mandelis, S. Buddhudu, and M. Kokta, "Photopyroelectric deconvolution of bulk and surface optical absorption and nonradiative energy conversion efficiency spectra in Ti:sapphire crystals," J. Appl. Phys. **75**, 8090–8097 (1994).
15. A. Mandelis, J. Vanniasinkam, S. Buddhudu, A. Othonos, and M. Kokta, "Absolute nonradiative energy-conversion-efficiency spectra in Ti:sapphire crystals measured by noncontact quadrature photopyroelectric spectroscopy," Phys. Rev. B **48**, 6808–6821 (1993).
16. P. A. Schultz and S. R. Henion, "Liquid-nitrogen-cooled Ti:sapphire laser," IEEE J. Quantum Electron. **27**, 1039–1047 (1991).